Analytical Verification for Vibration Analysis Technique used in Determination of Cracking in Cantilever Beams

by Ehsan Sarfaraz* and Hamid R. Hamidzadeh†

ABSTRACT

A nondestructive experimental technique for determination of structural discontinuities in cantilever beams is presented. The proposed technique is capable of detecting the location of cracks and other possible structural discontinuities on a beam using its first two natural frequencies measured by an accelerometer on a movable mass on the beam at several locations along the beam. To verify the validity of the proposed technique, the vibration response of a cracked cantilever beam with a stationary roving mass was investigated. The beam was modeled as an Euler-Bernoulli beam with a rectangular cross-section. The axial and transverse deformations of the cracked beam were coupled through a stiffness matrix determined using fracture mechanics principles. The developed model was used to determine analytical solutions for the variation of natural frequencies and mode shapes of a cracked cantilever beam versus the position of the roving mass. The analysis indicates that the variation of the natural frequencies versus position of the roving mass can drastically change when the roving mass is close to the position of a discontinuity. Moreover, the effects of the location and depth of the crack, as well as the location and weight of the roving mass, on the natural frequencies and mode shapes of the beam were investigated. The analytical results show that the coupling between the axial and transverse vibrations for moderate values of crack depth or roving mass is weak. Increasing the crack depth, the mass and the rotary inertia increases the coupling effect.

KEYWORDS: beam crack, crack detection, natural frequencies, mode shapes.

* Department of Mechanical and Manufacturing Engineering, Tennessee State University, 3500 John A. Merritt Blvd., Nashville, Tennessee 37209; (615) 963-5387; fax (615) 963-5496; e-mail esarfara@my.tnstate.edu.

† Department of Mechanical and Manufacturing Engineering, Tennessee State University, 3500 John A. Merritt Blvd., Nashville, Tennessee 37209; (615) 963-5387; fax (615) 963-5496; e-mail hhamidzadeh@tnstate.edu.

Introduction

Beams are one of the more commonly used structural elements in various engineering applications. They are often subjected to a wide variety of static and dynamic loads. Damages in such structures and applications are commonly due to cracks. One or more cracks in a beam could seriously influence the beam's dynamic characteristics. Some of the impacts of cracks in a beam are increased flexibility, a reduction in the natural frequencies, and altered vibration mode shapes. There are several works in literature on crack detection (ranging from the size to the location of the crack) in the structure using various techniques (Choi and Stubbs, 2004; Hadjileontiadis et al., 2005; Lu and Gao, 2005; Parloo et al., 2004; Zhong et al., 2008). There are also other research works on how the loading conditions and the crack affect the dynamic response of the structural performance (Dado and Abuzeid, 2003; Dong et al., 2004; Lin and Chang, 2006; Mahmoud and Abou Zaid, 2002; Zhong and Oyadiji, 2008).

One such study investigated the transverse vibration of cracked shafts in which the researchers computed the local flexibility due to the crack based on linear elastic fracture mechanics (Dimarogonas and Papadopoulos, 1983). Later, the work was extended to the coupled longitudinal and bending vibrations of cracked shafts (Papadopoulos and Dimarogonas, 1998). Two other works studied the vibrations of cracked beams with simply supported and cantilever boundary conditions (Chondros and Dimarogonas, 1998; Chondros et al., 1998). Results for the local flexibility technique were compared with the experimental results, and the observed results were in good agreement. Another work studied the coupling effects between the axial load and the crack depth of a cracked beam with fixed ends; it was found that the significance of the coupling effect was directly proportional to the axial load and the depth of the crack (Masoud et al., 1998).

It should be noted that vibration of a beam carrying a concentrated mass at an arbitrary location was studied previously (Low, 1999). The non-dimensional frequency response of the system was determined by solving the equations of motion and by imposing the corresponding boundary and compatibility conditions. The computed results showed an excellent agreement with the available experiment results. A later work studied the vibration response of cracked cantilever beams with an end mass including its rotary inertia and considered the coupling effect between axial and transverse deformation (Dado and Abuzeid, 2003). Another study investigated the dynamic response of cracked cantilever beams under a moving load and presented numerical results for different crack sizes, crack locations and different load speeds (Lin and Chang, 2006). Yet another work used an iterative modal analysis approach to get the dynamic response of a cracked simply supported beam subjected to a moving mass (Mahmoud and Zaid, 2002). A later work obtained an analytical solution of natural frequencies of cracked simply supported beams with a stationary roving mass (Zhong and Oyadiji, 2008). The effect of the crack was represented by a discontinuity or change in the slope of the beam at the crack location. A fracture mechanics technique was used to obtain the flexibility constant, which connects the change of the slope and the moment of the beam.

In this work, the vibration responses of a cracked cantilever beam with a stationary mass at numerous locations along the beam were investigated. The beam was modeled as an Euler-Bernoulli beam. The concentrated mass was modeled by introducing boundary conditions such that the deformations at the two sides of the mass had to satisfy the compatibility requirements. The crack was modeled by massless springs with sectional flexibility. The transverse deformation and axial deformation of the cracked beam were coupled in a stiffness matrix, which was determined based on fracture mechanics. The analytical solutions were obtained for the natural frequencies and mode shapes. The effects of the location and depth of the crack, as well as the location and the mass of the roving mass on the natural frequencies and mode shapes of the beam were also investigated. The presented analysis was made to verify the viability of a nondestructive experimental vibration technique to determine the position of possible discontinuities within the cantilever beams.

Formulation of a Cantilever Beam with an Open Crack

Consider a cracked cantilever beam with a block, as shown in Figure 1, where the mass of the block is m, and its rotary inertia about the neutral axis of the cross-section of the beam is J. The crack in the beam is assumed to be in the transverse direction with a depth of h_c. As depicted in Figure 1, L_m, L_c and L represent the distance from the left end (clamped end) of the beam to the location of the concentrated mass, the position of the crack, and the right end of the beam, respectively. The cross-section of the beam is rectangular, with a

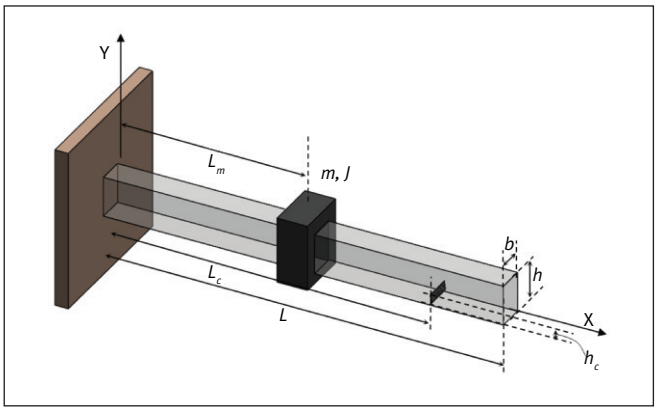

Figure 1. A cracked cantilever beam with auxiliary mass and rotary inertia.

width of b and a height of h. It was assumed that the material of the beam is linear elastic, and the crack always remains open during vibration so that the complexities associated with the nonlinear characteristics will be neglected (Chondros et al., 2001).

In this work, both axial and transverse vibrations are considered. The equation that governs the axial vibration of the beam can be expressed as:

$$\frac{\partial^2 u}{\partial x^2} - \frac{\rho}{E}\frac{\partial^2 u}{\partial t^2} = 0 \tag{1}$$

where

$u(x,t)$ is the axial displacement of a point in the beam,
ρ is the material density,
E is the Young's modulus (Weaver et al., 1990).

By using Euler-Bernoulli beam theory, the equation that governs the transverse vibration of the beam can be expressed as:

$$\frac{\partial^4 v}{\partial x^4} + \frac{\rho A}{EI}\frac{\partial^2 v}{\partial t^2} = 0 \tag{2}$$

where

$v(x,t)$ is the transverse displacement of the beam,
A is the beam's cross-section area,
I is the second moment of area for the cross-section with respect to its neutral axis (Biggs, 1964).

Considering that free vibration is harmonic, then the axial and transverse displacements can be written as Equations 3 and 4.

$$u(x,t) = U(x)\exp(i\omega t) \tag{3}$$

$$v(x,t) = V(x)\exp(i\omega t) \quad (4)$$

The spatial domains of the governing equations are given by Equations 5 and 6.

$$\frac{d^2U}{d\bar{x}^2} + k_u^2 U = 0 \quad (5)$$

$$\frac{d^4V}{d\bar{x}^4} - k_v^4 V = 0 \quad (6)$$

It should be noted that both U and V are functions of the non-dimensional variable of $\bar{x} = x / L$, and k_u and k_v are defined as Equations 7 and 8.

$$k_u^2 = \frac{\rho A L^2 \omega^2}{EA} \quad (7)$$

$$k_v^4 = \frac{\rho A L^4 \omega^2}{EI} \quad (8)$$

Note that both k_u and k_v are directly related to the natural frequency of the beam, ω.

The general solutions for differential Equations 5 and 6 are well known. For the cantilever beam model shown in Figure 1, the beam may be divided into three segments, and the general solutions of U and V for each segment can be written as follows.

For the first segment, $0 < \bar{x} < x_m$ (where $x_m = L_m / L$).

$$U_1(\bar{x}) = A_1 \cos(k_u \bar{x}) + A_2 \sin(k_u \bar{x}) \quad (9)$$

$$V_1(\bar{x}) = A_3 \cos(k_v \bar{x}) + A_4 \sin(k_v \bar{x}) + A_5 \cosh(k_v \bar{x}) + A_6 \sinh(k_v \bar{x}) \quad (10)$$

For the second segment, $x_m < \bar{x} < x_c$ (where $x_c = L_c / L$).

$$U_2(\bar{x}) = A_7 \cos(k_u \bar{x}) + A_8 \sin(k_u \bar{x}) \quad (11)$$

$$V_2(\bar{x}) = A_9 \cos(k_v \bar{x}) + A_{10} \sin(k_v \bar{x}) + A_{11} \cosh(k_v \bar{x}) + A_{12} \sinh(k_v \bar{x}) \quad (12)$$

For the third segment, $x_c < \bar{x} < 1$:

$$U_3(\bar{x}) = A_{13} \cos(k_u \bar{x}) + A_{14} \sin(k_u \bar{x}) \quad (13)$$

$$V_3(\bar{x}) = A_{15} \cos(k_v \bar{x}) + A_{16} \sin(k_v \bar{x}) + A_{17} \cosh(k_v \bar{x}) + A_{18} \sinh(k_v \bar{x}) \quad (14)$$

where

A_1 through A_{18} are arbitrary constants that can be determined by the boundary conditions and the compatibility conditions at the concentrated mass location and the crack location.

The boundary conditions at the fixed end of the cantilever beam (see Figure 1) require the axial and transverse displacements, as well as the slope of the transverse displacements, to be zero.

$$U_1(0) = 0,\ V_1(0) = 0,\ V_1'(0) = 0 \quad (15)$$

Similarly, for the free end of the beam, axial strain, shear force and bending moments are required to be zero.

$$U_3'(1) = 0,\ V_3''(1) = 0,\ V_3'''(1) = 0 \quad (16)$$

At the location of the concentrated mass and rotary inertia, $x = x_m$, the compatibility requirements enforce the continuity of axial and transverse the displacement components and the slope, such as in Equation 17.

$$U_1(x_m) = U_2(x_m),\ V_1(x_m) = V_2(x_m),\ V_1'(x_m) = V_2'(x_m) \quad (17)$$

The discontinuity in the forces and moment due to the presence of the concentrated mass gives:

$$U_2'(x_m) - U_1'(x_m) = -m_r k_u^2 U_1(x_m) \quad (18)$$

$$V_2''(x_m) - V_1''(x_m) = J_r k_v^4 V_1'(x_m) \quad (19)$$

$$V_2'''(x_m) - V_1'''(x_m) = m_r k_v^4 V_1(x_m) \quad (20)$$

where

m_r and J_r are, respectively, the mass ratio and rotary inertia ratio, and are given by Equation 21.

$$m_r = \frac{m}{\rho A L}, \text{ and } J_r = \frac{J}{\rho A L^3} \quad (21)$$

The presence of a transverse crack in the beam reduces its stiffness. Thus, the crack may be modeled as an extensional spring, a rotational spring or both. The number of springs needed depends on the degrees of freedom considered. As both axial and transverse vibrations of the beam were considered, the crack was modeled as both an extensional spring and a rotational spring.

At the crack location, $\bar{x} = x_c$, the compatibility requirements can be expressed using the model used in outside work (Dado and Abuzeid, 2003; Loya et al., 2006).

$$(22)\quad U_2'(x_c) = U_3'(x_c)$$

$$(23)\quad V_2(x_c) = V_3(x_c),\ V_2''(x_c) = V_3''(x_c),\ V_2'''(x_c) = V_3'''(x_c)$$

The axial force, P, and the bending moment, M, at the crack may be expressed as:

$$(24)\quad \begin{Bmatrix} P \\ M \end{Bmatrix} = \begin{bmatrix} k_{11} & k_{12} \\ k_{21} & k_{22} \end{bmatrix} \begin{Bmatrix} U_3(x_c) - U_2(x_c) \\ V_3'(x_c) - V_2'(x_c) \end{Bmatrix}$$

where

k_{ij} are the elements of the stiffness matrix, including the functions of the crack depth, cross-section geometry of the beam, and the material properties.

The derivations of these elements are given in the Appendix. On the other hand, P and M can be expressed by the deformation components as in Equation 25.

$$(25)\quad \begin{Bmatrix} P \\ M \end{Bmatrix} = \begin{Bmatrix} EAU_2'(x_c) \\ EIV_2''(x_c) \end{Bmatrix}$$

Combining Equations 22 and 23 gives Equation 26.

$$(26)\quad \begin{Bmatrix} EAU_2'(x_c) \\ EIV_2''(x_c) \end{Bmatrix} = \begin{bmatrix} k_{11} & k_{12} \\ k_{21} & k_{22} \end{bmatrix} \begin{Bmatrix} U_3(x_c) - U_2(x_c) \\ V_3'(x_c) - V_2'(x_c) \end{Bmatrix}$$

There are 18 equations, that is, Equations 15–20, 22, 23 and 26, which define a set of 18 homogeneous linear simultaneous algebraic equations with A_1 to A_{18} as variables. These equations may be written in matrix form as:

$$(27)\quad [\mathbf{B}]\{\mathbf{A}\} = \{\mathbf{0}\}$$

where

$\{\mathbf{A}\} = [A_1\ A_2\ A_3\ \ldots\ A_{18}]^T$ is a vector of variables,

$[B]$ is an 18×18 matrix whose elements are determined by those 18 equations.

Note that some of the elements of $[B]$ contain natural frequency ω.

The natural frequencies of the vibration of the cantilever beam are determined by letting the determinant of $[B]$ be zero, as in Equation 28.

$$(28)\quad \det[\mathbf{B}] = 0$$

For a natural frequency obtained from Equation 28, the associated mode shape can be obtained by solving Equation 27 for $A_1\ A_2\ A_3\ \ldots\ A_{18}$. By choosing the value of one of the variables as unit (for example, let $A_1 = 1$), all other values of A can be found from Equation 27. Once these constants are determined, they can be substituted back into Equations 9 to 14 to determine the mode shape.

Numerical Results and Discussions

To compute the first two natural frequencies of the system, the first two roots of nonlinear algebraic Equation 28 have to be determined. Computations of roots of Equation 28 for two different cases were conducted using the fsolve function in commercial software (MathWorks, 2011). The first case considered the transverse vibration of a cantilever beam with a concentrated mass attached at the free end. It was assumed that the beam was made of bright mild steel with a Young's modulus of 210 GPa and mass density of 7850 kg/m^3. The length, width and height of the beam were assumed to be 3000, 100 and 25 mm, respectively. Using the Euler-Bernoulli beam theory, one could determine the analytical solution for the natural frequency as a function of the mass ratio of the concentrated mass to the mass of the beam. Table 1 presents excellent agreement between numerical results for the first two natural frequencies of a beam with a concentrated mass at the free end and those of the presented model when the concentrated mass was located at the free end (Rao, 2007). Furthermore, the computed percentage of errors presented in Table 1 verifies the validity of the presented approach. It should be noted that the analytical solution presented in the table is also a numerical solution for the reason that the resulting equation for the natural frequency is a nonlinear equation (Rao, 2007). Because of the presented modeling of the crack, the formulation introduced in this paper would not automatically reduce to the governing equation for a whole beam, as the crack depth approaches zero.

The second case study considered a cantilever beam with a transverse crack, where the beam was 300 mm long and had a square cross-section with side length of 20 mm. In this case, the crack was located at the position of 140 mm away from the fixed end, and had a depth of 10 mm. Furthermore, the Young's modulus for the beam was 206 GPa, and its mass density was 7800 kg/m^3. The first three natural frequencies were computed, and the results were compared with the numerical and experimental results obtained by outside researchers (Lin and Chang, 2006; Rizos and Asparagathos, 1990). The comparison of the natural frequencies and the computed percentage of errors are presented in Table 2. This table demonstrates that the results of this study are in a good agreement with the experimental results for the examined cracked cantilever beam.

TABLE 1
Comparison of natural frequencies between analytical solution and numerical solution for a cantilever beam with a concentrated mass at the free end

$m_r = m / (\rho AL)$	ω_1 (rad/s)			ω_2 (rad/s)		
	theory	present results	% error	theory	present results	% error
0	14.58	14.58	0	91.39	91.39	0.01
0.005	14.44	14.44	0	90.50	90.51	0.01
0.01	14.30	14.30	0	89.67	89.68	0.01
0.03	13.78	13.78	0	86.78	86.79	0.01
0.05	13.31	13.31	0	84.46	84.47	0.01
0.07	12.88	12.88	0	82.56	82.57	0.01
0.1	12.31	12.31	0	80.30	80.29	0.01
0.5	8.36	8.36	0	70.10	70.11	0.01
1	6.46	6.46	0	67.39	67.41	0.03
2	4.80	4.80	0	65.78	65.79	0.01
3	3.99	3.99	0	65.20	65.21	0.01
4	3.49	3.49	0	64.90	64.91	0.01
5	3.14	3.14	0	64.71	64.72	0.01
10	2.25	2.25	0	64.33	64.35	0.03
100	0.72	0.72	0	63.99	64.00	0.01

TABLE 2
Comparison of natural frequencies for a cracked cantilever beam

Frequency (rad/s)	Experiment	Prior study		Present results	
		computed	% error	computed	% error
ω_1	1074	1095	1.955	1096	2.048
ω_2	6202	6201	0.016	6242	0.645
ω_3	19063	20217	6.054	20148	5.692

The effects of the crack and concentrated mass on the vibration response of the cantilever beam are examined in the following section. The beam's geometrical and material properties were the same as the aforementioned case study. The effects of the crack are examined first, followed by the effect of mass and the combined effect of crack and concentrated mass.

Effect of the Crack on the Natural Frequencies

The effects of the crack depth (non-dimensional parameter h_c / h) and its location (non-dimensional parameter L_c / L) on the first two natural frequencies, ω_1 and ω_2, were examined. Figure 2 shows the 3D plots of normalized natural frequencies versus h_c / h and L_c / L for non-dimensional mass ratio, $m_r = 0$, $m_r = 0.05$ and $m_r = 0.5$, at a fixed point $L_m / L = 0.45$. The two frequencies were normalized by dividing them by their counterpart of the intact beam, that is, $\omega_{10} = 14.58$ (rad/s) and $\omega_{20} = 91.39$ (rad/s).

As illustrated, the general trends for changes in the first two natural frequencies for different possible positions of a crack and a wide range of crack depth ratios for three different mass ratios in three cases were shown. In fact, the main scope of the presented graphs was to draw a conclusion for the general trend of these frequencies. From the presented results, it was observed that the presence of the concentrated mass did not alter the patterns of either natural frequency. In fact, the natural frequencies decreased as the ratio m_r increased. For the values of m_r from zero up to 0.5, when the crack depth was $h_c / h < 0.50$, the crack did not have a significant effect on the natural frequencies. It was estimated that, for the range of values of h_c / h from 0 to 0.50, the maximum difference for both natural frequencies was no more than 3.5%. It was shown, as the crack depth increases, both natural frequencies decrease; however, that effect is strongly dependent on the crack location. The effect of the crack location on the two natural frequencies is different. For the first natural frequency, the closer the crack is to the fixed end of the beam, the greater it affects the frequency; while for the second natural frequency, the most critical effect occurred when the crack was around the mid-span of the beam. The next severe effect occurred when the crack was near the fixed end of the beam. For both frequencies, the crack effect diminished as the crack neared the free end of the cantilever beam.

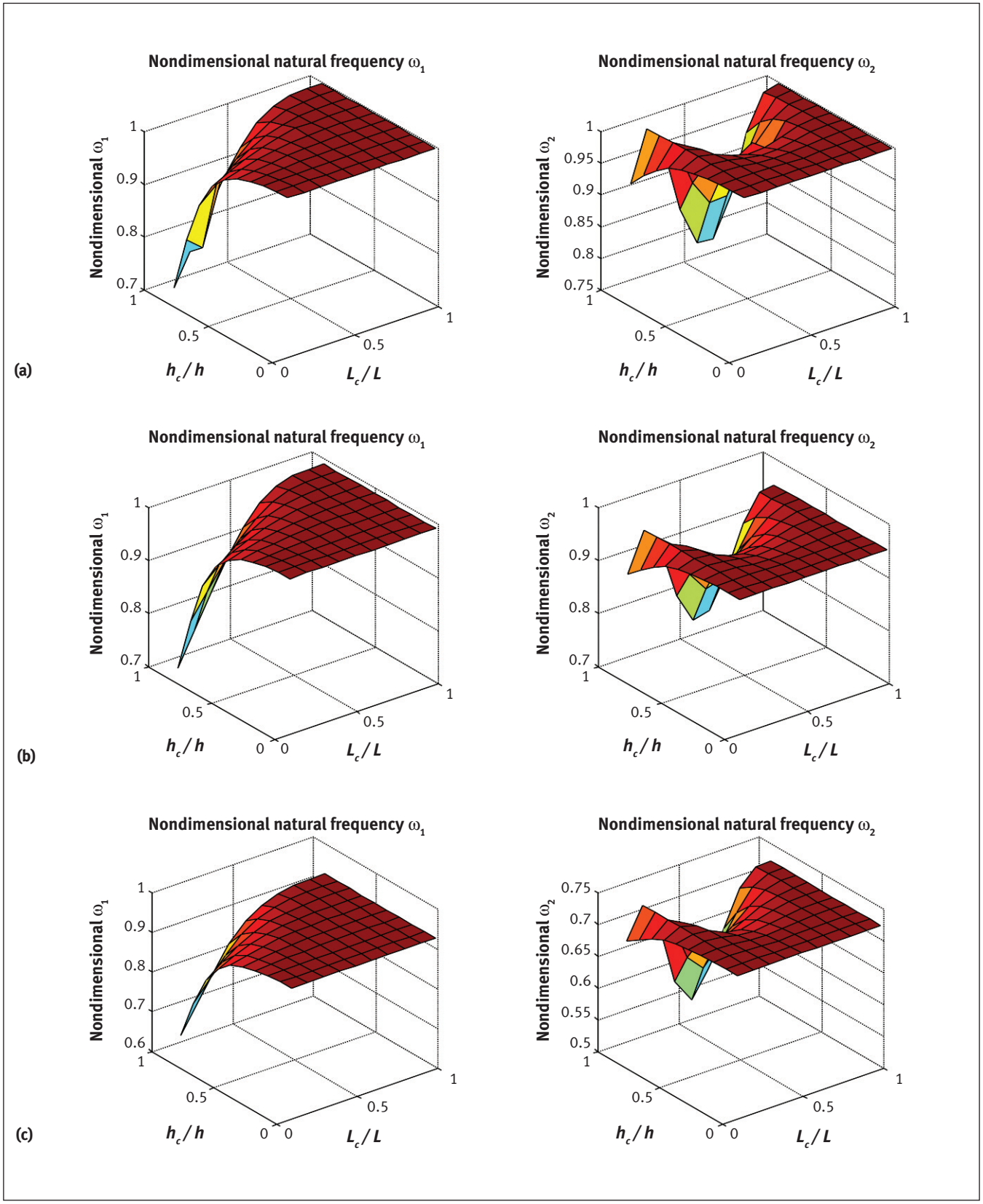

Figure 2. Variation of the first two normalized natural frequencies versus L_c / L and h_c / h for different mass ratios of m_r = 0.0, 0.05 and 0.5: (a) for case 1, m_r = 0; (b) for case 2, m_r = 0.05; and (c) for case 3, m_r = 0.5.

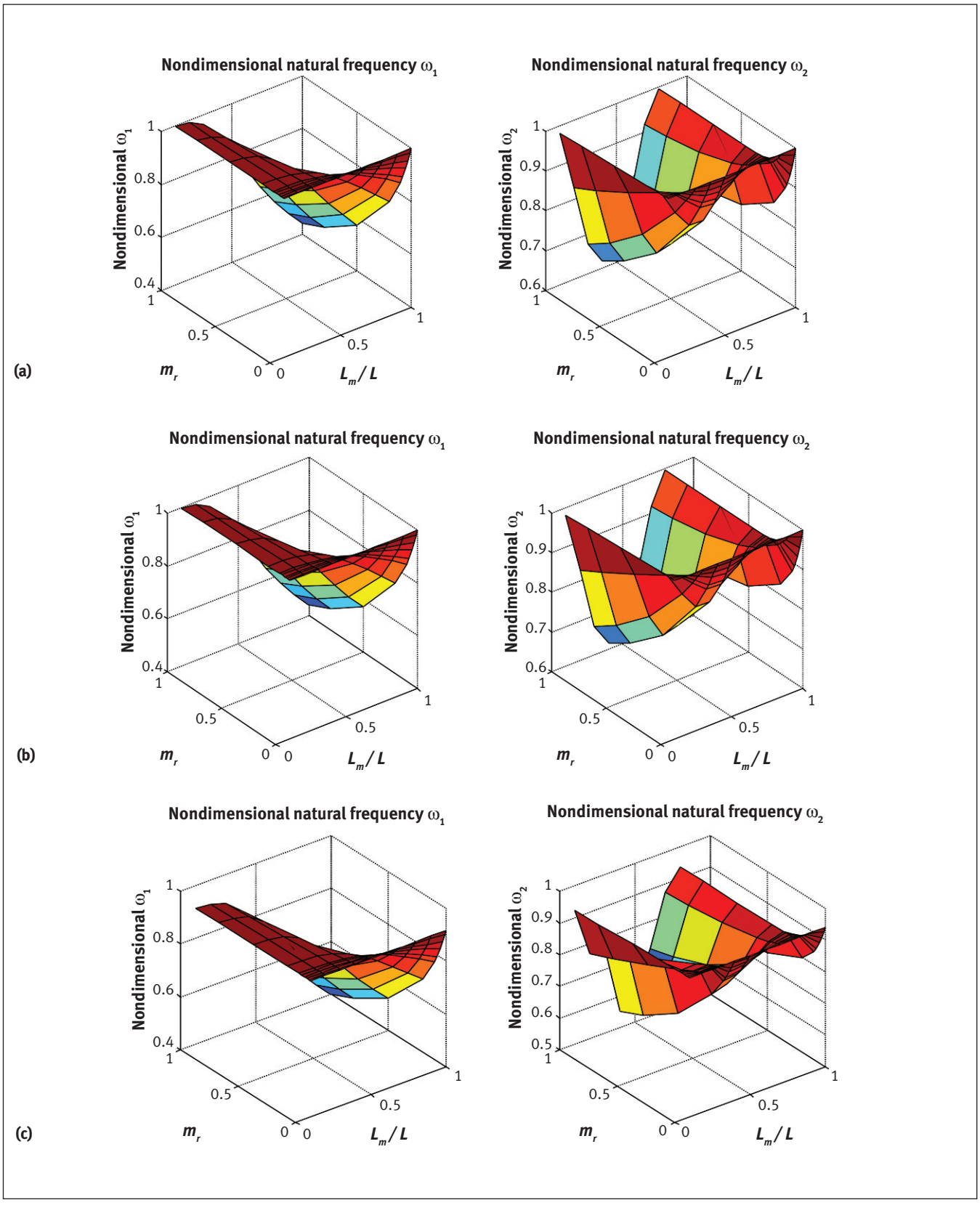

Figure 3. Variation of the first two normalized natural frequencies versus concentrated mass and its location for three different values of h_c / h = 0.0, 0.2 and 0.8: (a) for case 1, h_c / h = 0; (b) for case 2, h_c / h = 0.2; and (c) for case 3, h_c / h = 0.8.

TABLE 3
Natural frequencies versus L_m / L for a cantilever beam (m_r = 0.8 and L_c / L = 0.35)

L_m / L	ω_1 (rad/s)			ω_2 (rad/s)		
	h_c / h = 0	h_c / h = 0.2	h_c / h = 0.8	h_c / h = 0	h_c / h = 0.2	h_c / h = 0.8
0.001	14.58	14.56	13.35	91.39	91.28	85.86
0.05	14.58	14.56	13.35	91.29	91.18	85.76
0.10	14.58	14.55	13.35	90.07	89.96	84.51
0.15	14.55	14.53	13.33	85.87	85.76	80.21
0.20	14.48	14.46	13.29	78.65	78.52	72.78
0.25	14.36	14.34	13.21	71.08	70.94	64.72
0.30	14.15	14.14	13.07	65.19	65.03	57.94
0.35	13.85	13.83	12.87	61.44	61.24	52.83
0.40	13.45	13.43	12.50	59.70	59.57	53.48
0.45	12.96	12.94	12.03	59.80	59.71	55.03
0.50	12.41	12.39	11.50	61.64	61.56	57.72
0.55	11.82	11.80	10.92	65.18	65.11	61.72
0.60	11.20	11.19	10.33	70.46	70.39	67.09
0.65	10.60	10.58	9.74	77.27	77.20	73.63
0.70	10.00	9.99	9.17	84.68	84.59	80.33
0.75	9.44	9.42	8.63	90.21	90.10	84.96
0.80	8.90	8.88	8.12	91.11	91.00	85.60
0.85	8.39	8.38	7.64	87.53	87.43	82.68
0.90	7.91	7.90	7.19	81.54	81.46	77.78
0.999	7.06	7.05	6.40	68.26	68.22	66.46

Effects of the Concentrated Mass on the Natural Frequencies

The effect of the concentrated mass and its location on the natural frequencies of the cracked beam was examined. Figure 3 shows the 3D plots of the normalized first two natural frequencies versus m_r and L_m / L for h_c / h = 0, 0.2 and 0.8, respectively. The crack was assumed to be located at a fixed point of L_c / L = 0.35.

Figure 3 illustrates the results of an intact cantilever beam carrying a mass. When m_r = 0, $\omega_1 = \omega_{10}$ = 14.58 (rad/s) and $\omega_2 = \omega_{20}$ = 91.39 (rad/s). When $m_r \neq 0$, ω_1 decreases as the concentrated mass increases. ω_1 also decreases as the mass is placed away from the fixed end of the beam. ω_2 is affected by the concentrated mass in a different way; it reduces significantly the value of ω_2 as it is moving away from the fixed end of the beam to the center of the beam. The effect diminishes as it continues moving away from the center, and becomes significant again as nears the free end of the beam. Similar patterns were reported elsewhere (Low, 1994). In order to examine the effect of the crack length on the frequencies, the first two natural frequencies against L_m / L were computed, and the results are given in Table 3. The normalized frequencies ω_1 and ω_2 versus L_m / L are plotted in Figure 4, respectively. In both cases, m_r = 0.8, and the crack was assumed to be located at L_c / L = 0.35. These results show that the presence of a crack in the beam does not alter the frequency patterns; it only amplifies them.

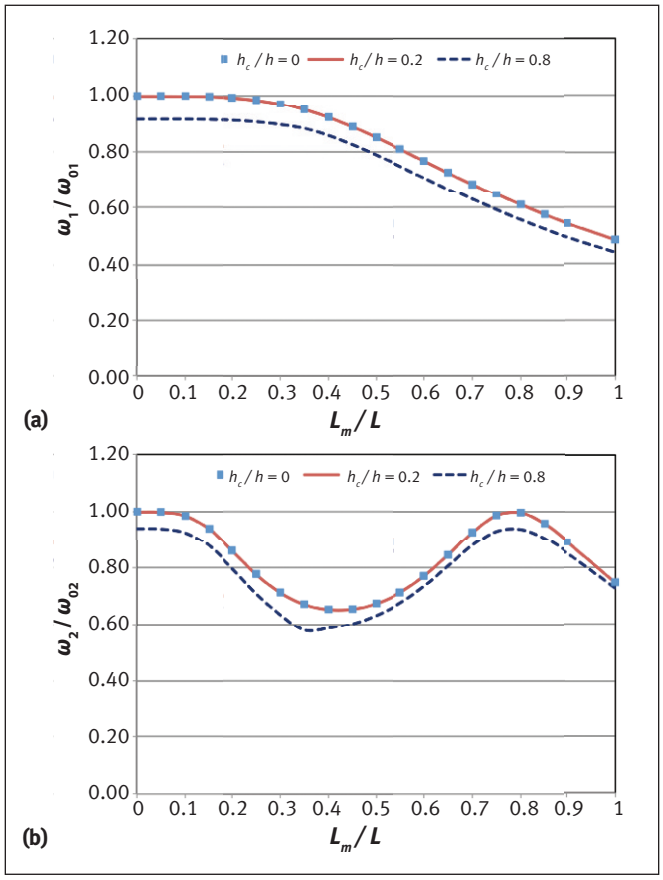

Figure 4. Normalized natural frequencies versus L_m / L for m_r = 0.8 and L_c / L = 0.35 for three different values of h_c / h.

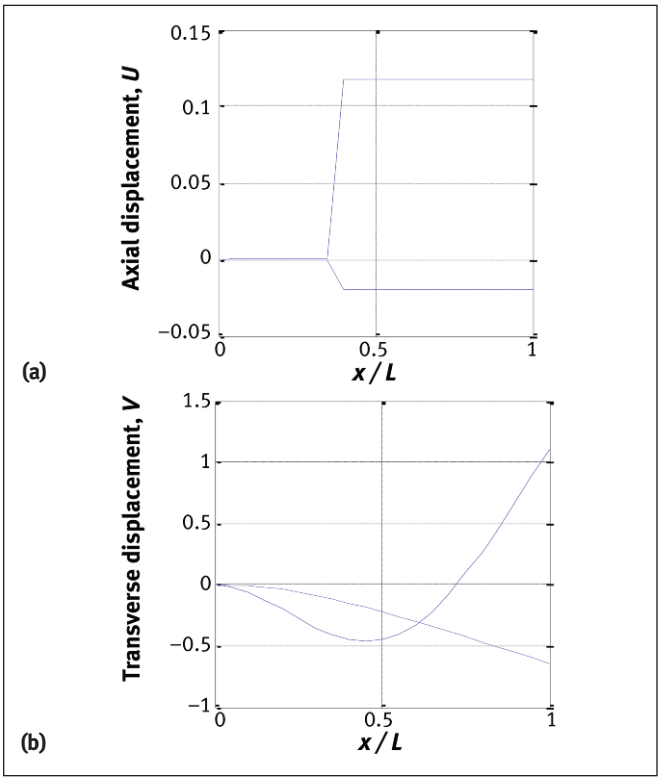

Figure 5. The first two mode shapes of cracked beam for L_m / L = 0.6 and L_c / L = 0.35, where ω_1 = 11.2 (rad/s) and ω_2 = 70.9 (rad/s): (a) axial displacements; and (b) transverse displacements.

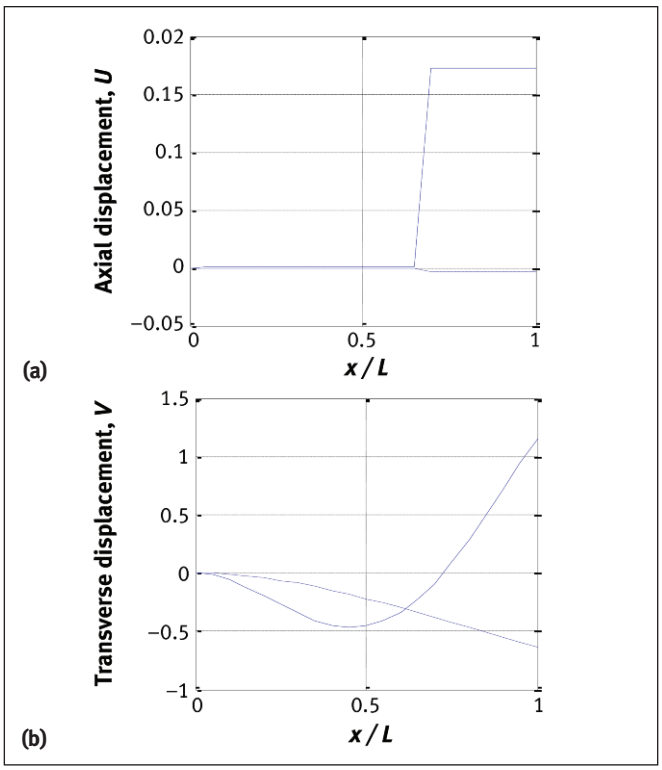

Figure 6. The first two mode shapes of cracked beam for L_m / L = 0.6 and L_c / L = 0.70, where ω_1 = 12.1 (rad/s) and ω_2 = 66.9 (rad/s): (a) axial displacements; and (b) transverse displacements.

Analysis of Mode Shapes

The numerical results show that, for intact beams, the axial displacement $U(x)$ is insignificant. However, for cracked beams, $U(x)$ is in general much smaller than $V(x)$. It should be noted that $U(x)$ varies as a sine function with a very small (almost flat) value, along the longitudinal direction of the beam. Its value has a relatively big change across the crack and then becomes flat again. The transverse displacement $V(x)$ is the dominant deformation, and the mode shapes of $V(x)$ are close to their counterpart of the intact cantilever beam without a concentrated mass. The coupling between $U(x)$ and $V(x)$ is dependent on the crack depth, and is very weak except for extremely deep crack depths. Figures 5 to 7 show the first two mode shapes for the three typical cases. For all the three cases, the mass ratio, m_r, is fixed at 0.5 and the crack depth ratio h_c / h is fixed at 0.5. The difference among these cases is the relative position of the crack, and the concentrated mass. Note that the U and V values in these figures do not reflect the real deformation of these problems.

Detection of Crack Location

For simply supported beams, a recent study proposed a frequency-domain approach to detect the damage location (Zhong and Oyadiji, 2009). For an aluminum beam, researchers used the finite element method combined with the spectral center correction technique to determine variation of the fundamental natural frequency versus position of

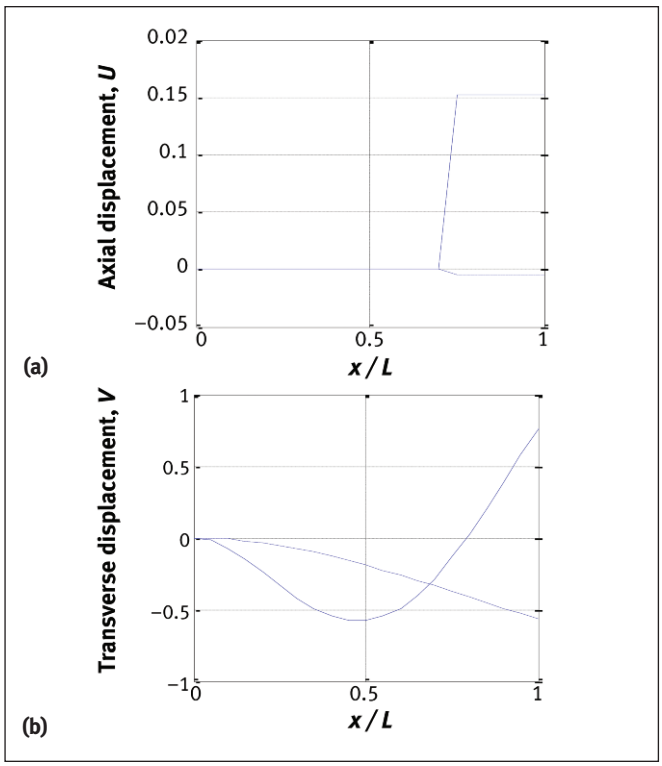

Figure 7. The first two mode shapes of cracked beam for L_m / L = 0.8 and L_c / L = 0.70, where ω_1 = 10.1 (rad/s) and ω_2 = 83.4 (rad/s): (a) axial displacements; and (b) transverse displacements.

the mass. They used derivatives of fundamental frequency with respect to the location of the mass to determine the location of a crack.

The same process is used here for the presented computed results for different cases. Figure 8a for case 1 presents the variation of dimensionless fundamental natural frequency of a cracked beam along with the first five derivatives of it with respect to the ratio of L_m / L, m_r = 0.8 and L_c / L = 0.35. Obviously, the second derivative curve clearly shows the location of the crack as it exhibits a sharp change of the curve.

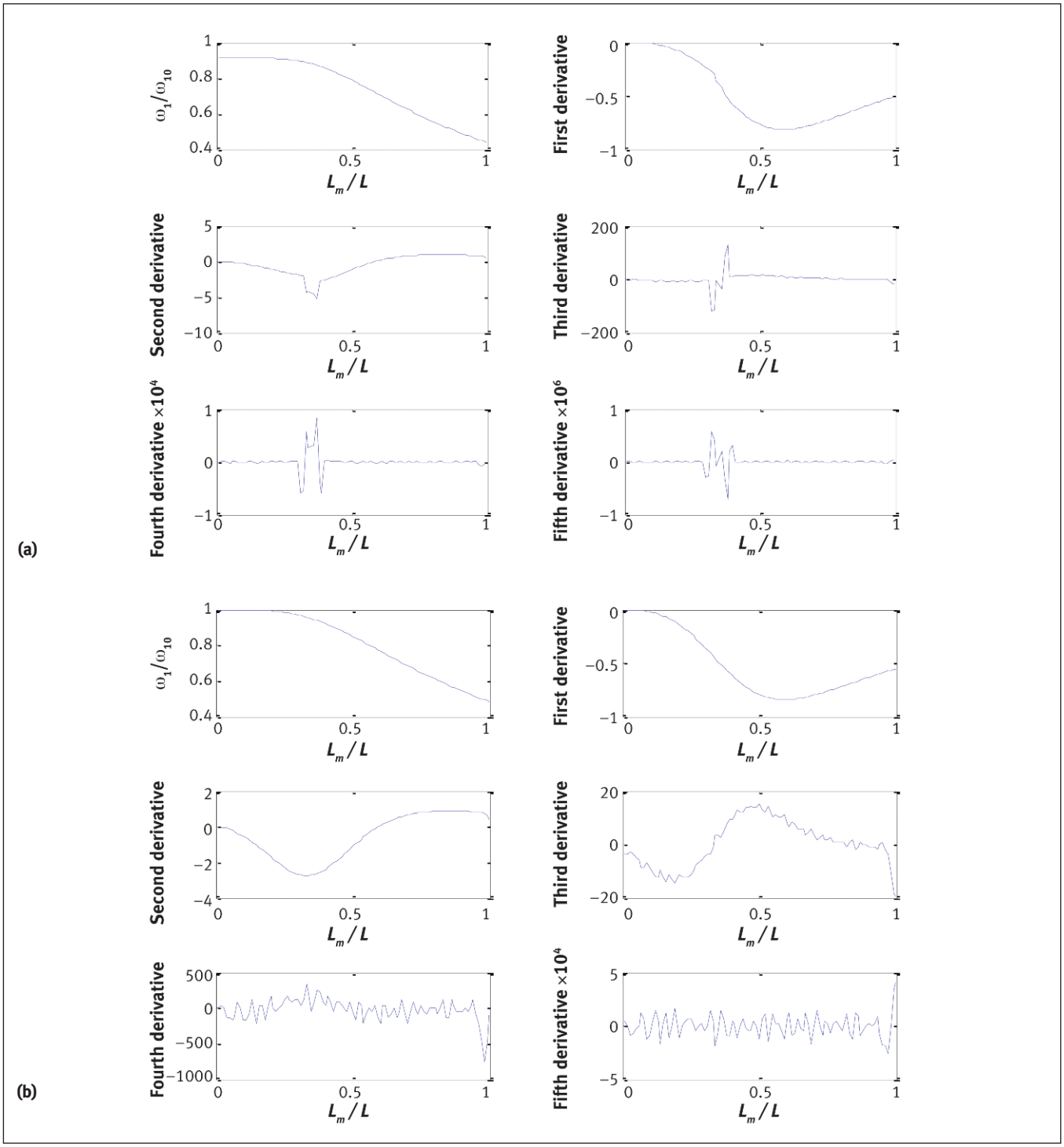

Figure 8. Normalized ω_1 and its derivatives with respect to L_m / L versus L_m / L for m_r = 0.8: (a) for case 1, L_c / L = 0.35; and (b) for case 2, L_c / L = 0.

For contrast, Figure 8b for case 2 shows the result for the same problem, except without a crack (that is, $L_c / L = 0$). Without a crack, the natural frequency and its derivative curves are all smooth. As demonstrated, the position of the crack is indicated by a sharp discontinuity in the second through fifth derivatives curves shown.

Conclusion

The vibration behavior of cracked cantilever beams under a roving stationary concentrated mass and rotary inertia was investigated. Both the axial and transverse deformations were considered. The continuous beam was divided into three segments by the concentrated mass and the crack. Vibration of each segment was analyzed by Euler-Bernoulli beam theory. The boundary conditions and the compatibility requirements at the joints of the segments were reinforced. The crack was modeled as elastic springs (one extensional and another rotational), and the stiffness matrix was obtained based on fracture mechanics.

The analytical results show that axial vibration is much smaller compared to the transverse vibration. For the first two modes, the coupling effect between the axial and transverse vibrations was weak. It was observed that both the concentrated mass and the crack reduced the natural frequencies, but the way they affected the frequency was different. Frequencies decreased as the concentrated mass or crack depth increased.

For the values of mass ratio, m_r, and the crack depth ratio, a/h, up to 0.5, the reduction of the first two natural frequencies was no more than 3.5%. The effect of the crack location on the two natural frequencies was different. As was expected for the first frequency, as the crack nears the fixed end of the beam, reduction of the frequency increased. For the second natural frequency, when the crack was around the mid-span of the beam, or the fixed end of the beam, the reduction of the frequency increased. For both frequencies, the crack effect diminished as the crack nears the free end of the cantilever beam. The location of the concentrated mass had a significant effect on the frequencies. For the first natural frequency, as the mass moved away from the fixed end of the beam to the free end of the beam, the reduction of the frequency increased. For the second natural frequency, the concentrated mass wound significantly reduced the frequency when it was around the center of the beam, or close to the free end of the beam. Furthermore, the second derivative of the first natural frequency curve is an effective indicator to show the location of the crack in the cantilever beam. The presented nondestructive experimental approach is capable of identifying the positions of separate discontinuities along the beam; however, the accuracy of the procedure can be enhanced by increasing the number of measurement points for the first two natural frequencies of the stationary roving mass along the beam. Based on the methodology presented here, a similar experimental procedure can be adopted to determine the location of discontinuities for a given specific structure by comparing the experimental results with similar data for a similar complex structure without discontinuities.

REFERENCES

Biggs, J.M., *Introduction to Structural Dynamics*, McGraw-Hill, New York, New York, 1964.

Choi, S. and N. Stubbs, "Damage Identification in Structures using the Time-domain Response," *Journal of Sound and Vibration*, Vol. 275, Nos. 3–5, 2004, pp. 577–590.

Chondros, T.G. and A.D. Dimarogonas, "Vibration of a Cracked Cantilever Beam," *Journal of Vibration and Acoustics*, Vol. 120, No. 3, 1998, pp. 742–746.

Chondros, T.G., A.D. Dimarogonas and J. Yao, "A Continuous Cracked Beam Vibration Theory," *Journal of Sound and Vibration*, Vol. 215, No. 1, 1998, pp. 17–34.

Chondros, T.G., A.D. Dimarogonas and J. Yao, "Vibration of a Beam with a Breathing Crack," *Journal of Sound and Vibration*, Vol. 239, No. 1, 2001, pp. 57–67.

Dado, M.H.F. and O. Abuzeid, "Coupled Transverse and Axial Vibratory Behavior of Cracked Beam with End Mass and Rotary Inertia," *Journal of Sound and Vibration*, Vol. 261, No. 4, 2003, pp. 675–696.

Dimarogonas, A.D. and C.A. Papadopoulos, "Vibration of Cracked Shafts in Bending," *Journal of Sound and Vibration*, Vol. 91, No. 4, 1983, pp. 583–593.

Dong, G.M., J. Chen and J. Zou, "Parameter Identification of a Rotor with an Open Crack," *European Journal of Mechanics – A/Solids*, Vol. 23, No. 2, 2004, pp. 325–333.

Hadjileontiadis, L.J., E. Douka and A. Trochidis, "Crack Detection in Beams using Kurtosis," *Computers and Structures*, Vol. 83, Nos. 12–13, 2005, pp. 909–919.

Lin, H.P. and S.C. Chang, "Forced Response of Cracked Cantilever Beams Subjected to a Concentrated Moving Load," *International Journal of Mechanical Sciences*, Vol. 48, No. 12, 2006, pp. 1456–1463.

Low, K.H., "Comparisons of Experimental and Numerical Frequencies for Classical Beams Carrying a Mass In-span," *International Journal of Mechanical Sciences*, Vol. 41, No. 12, 1999, pp. 1515–1531.

Loya, J.A., L. Rubio and J. Fernandez-Saez, "Natural Frequencies for Bending Vibrations of Timoshenko Cracked Beams," *Journal of Sound and Vibration*, Vol. 290, Nos. 3–5, 2006, pp. 640–653.

Lu, Y. and F. Gao, "A Novel Time Domain Auto-regressive Model for Structural Damage Diagnosis," *Journal of Sound and Vibration*, Vol. 283, 2005, pp. 1031–1049.

Mahmoud, M.A. and M.A. Abou Zaid, "Dynamic Response of a Beam with a Crack Subject to a Moving Mass," *Journal of Sound and Vibration*, Vol. 256, No. 4, 2002, pp. 591–603.

Masoud, S., M.A. Jarrah and M. Al-Maamory, "Effect of Crack Depth on the Natural Frequency of a Pre-stressed Fixed-fixed Beam," *Journal of Sound and Vibration*, Vol. 214, No. 2, 1998, pp. 201–212.

MathWorks, "Root of Nonlinear Function – MATLAB fzero," *Documentation Center*, MathWorks, Natick, Massachusetts, www.mathworks.com/help/matlab/ref/fzero.html, 2011.

Papadopoulos, C.A. and A.D. Dimarogonas, "Coupled Longitudinal and Bending Vibrations of a Cracked Shaft," *Journal of Vibration, Acoustics, Stress and Reliability in Design*, Vol. 110, No. 1, 1988, pp. 1–8.

Parloo, E., S. Vanlanduit, P. Guillaume and P. Verboven, "Increased Reliability of Referenced-based Damage Identification Techniques by using Output-only Data," *Journal of Sound and Vibration*, Vol. 270, Nos. 4–5, 2004, pp. 813–832.

Rao, S.S., *Vibration of Continuous Systems*, John Wiley & Sons, Hoboken, New Jersey, 2007.

Rizos, P.F. and N. Asparagathos, "Identification of Crack Location and Magnitude in a Cantilever Beam from the Vibrating Modes," *Journal of Sound and Vibration*, Vol. 138, No. 2, 1990, pp. 381–388.

Weaver, Jr., W., S.P. Timoshenko and D.H. Young, *Vibration Problems in Engineering*, 5th ed., John Wiley & Sons, New York, New York, 1990.

Zhong, S. and S.O. Oyadiji, "Analytical Prediction of Natural Frequencies of Cracked Simply Supported Beams with a Stationary Roving Mass," *Journal of Sound and Vibration*, Vol. 311, Nos. 1–2, 2008, pp. 328–352.

Zhong, S. and S.O. Oyadiji, "Response-only Frequency-domain Method for Structural Damage Detection," *ASME 2009 International Design Engineering Technical Conferences and Computers and Information in Engineering Conference*, 30 August–2 September 2009, San Diego, California, pp. 1–8.

Zhong, S., S.O. Oyadiji and K. Ding, "Response-only Method for Damage Detection of Beam-like Structures using High Accuracy Frequencies with Auxiliary Mass Spatial Probing," *Journal of Sound and Vibration*, Vol. 311, Nos. 3–5, 2008, pp. 1075–1099.

APPENDIX

The crack stiffness matrix was obtained as the inverse of the local flexibility matrix due to the crack, while the elements of the flexibility matrix were obtained as the second derivatives of the total energy release rate with respect to the individual loading parameters. For an Euler-Bernoulli beam with a transverse crack under axial force P and moment M, the mode I stress intensity factor can be expressed by using the superposition principle as:

$$K_I = \sqrt{2h\tan\frac{\pi\alpha}{2}}\left(\frac{P}{bh}F_1 + \frac{6M}{bh^2}F_2\right) \quad (29)$$

where

$\alpha = a / h$ is the non-dimensional crack depth,

b and h are the width and height of the cross-section of the beam,

F_1 and F_2 are functions of α and are given by Equations 30 and 31.

$$F_1 = \frac{0.752 + 2.02\alpha + 0.37\left(1 - \sin\frac{\pi\alpha}{2}\right)^3}{\cos\frac{\pi\alpha}{2}} \quad (30)$$

$$F_1 = \frac{0.923 + 0.199\left(1 - \sin\frac{\pi\alpha}{2}\right)^4}{\cos\frac{\pi\alpha}{2}} \quad (31)$$

Assuming the plane strain condition, the energy release rate is related to the stress intensity factor by:

$$G = \frac{1-\nu^2}{E}K_I^2 \quad (32)$$

where

E is the Young's modulus,

ν is the Poisson's ratio.

The local flexibility matrix elements are given by:

$$c_{11} = \frac{\partial^2}{\partial P^2}\int_0^{h_c} bG\,da = \frac{4\left(1-\nu^2\right)}{Eb}\int_0^{h_c/h}\tan\frac{\pi\alpha}{2}F_1^2(\alpha)\,d\alpha \quad (33)$$

$$c_{12} = c_{21} = \frac{\partial^2}{\partial P\partial M}\int_0^{h_c} bG\,da = \frac{24\left(1-\nu^2\right)}{Ebh}\int_0^{h_c/h}\tan\frac{\pi\alpha}{2}F_1(\alpha)F_2(\alpha)\,d\alpha \quad (34)$$

$$c_{22} = \frac{\partial^2}{\partial M^2}\int_0^{h_c} bG\,da = \frac{144\left(1-\nu^2\right)}{Ebh^2}\int_0^{h_c/h}\tan\frac{\pi\alpha}{2}F_2^2(\alpha)\,d\alpha \quad (35)$$

where

h_c is the maximum crack depth.

The integrals in Equations 33 through 35 were evaluated numerically using a 16-point Gauss quadrature formula. The results were then fitted to polynomial expressions with $\bar{a} = h_c / h$ as the variable. The flexibility matrix elements are found as Equations 36, 37 and 38.

$$c_{11} = \frac{4\left(1-\nu^2\right)}{Eb}\left(0.0090175 + 0.157641\bar{a} - 6.49871\bar{a}^2 + 55.21691\bar{a}^3 - 139.55434\bar{a}^4 + 130.56115\bar{a}^5\right) \quad (36)$$

$$c_{12} = c_{21} = \frac{24\left(1-\nu^2\right)}{Ebh}\left(0.00334625 + 0.059966\bar{a} - 1.82871\bar{a}^2 + 20.03677\bar{a}^3 - 50.91214\bar{a}^4 + 48.91571\bar{a}^5\right) \quad (37)$$

$$c_{22} = \frac{144\left(1-\nu^2\right)}{Ebh^2}\left(0.00083865 + 0.040585\bar{a} - 0.28828\bar{a}^2 + 7.06450\bar{a}^3 - 18.36010\bar{a}^4 + 18.18070\bar{a}^5\right) \quad (38)$$

Therefore, the stiffness matrix is given by Equation 39.

$$\begin{bmatrix} k_{11} & k_{12} \\ k_{21} & k_{22} \end{bmatrix} = \begin{bmatrix} c_{11} & c_{12} \\ c_{21} & c_{22} \end{bmatrix}^{-1} \quad (39)$$